Research Square

Preprints are preliminary reports that have not undergone peer review.
They should not be considered conclusive, used to inform clinical practice,
or referenced by the media as validated information.

Integrating Sentinel-1 backscatter and co-occurrence texture metrics for vegetation fuel classification

Thiare Vildo
Pontificia Universidad Católica de Chile
Erico Kutchartt
Joint Research Unit CTFC – AGROTECNIO
Horacio Gilabert
Pontificia Universidad Católica de Chile
Felipe La Barra
Complex Engineering System Institute (ISCI)
Francesco Pirotti
University of Padova
Marcelo D. Miranda
mmirands@uc.cl

Pontificia Universidad Católica de Chile

Research Article

Keywords: Active sensors, Haralick, Machine learning, Fire prevention, Mediterranean ecosystems

Posted Date: November 5th, 2026

DOI: https://doi.org/10.21203/rs.3.rs-10681478/v1

License: This work is licensed under a Creative Commons Attribution 4.0 International License.
Read Full License

Additional Declarations: No competing interests reported.

Abstract

Wildfires have increased in frequency and severity across the Mediterranean ecosystems of central Chile, emphasizing the need for accurate vegetation fuel mapping to support wildfire risk assessment and management. This study evaluated the potential of Sentinel-1 Synthetic Aperture Radar (SAR) imagery to discriminate vegetation fuel classes defined by the Chilean KITRAL fuel classification system. A total of 3,645 reference polygons were delineated through detailed photo-interpretation and subsequently validated by field surveys to classify four fuel classes: native forest, forest plantation, shrubland, and grassland. Three Sentinel-1 backscatter variables (VV, VH, and the VV/VH ratio) and Haralick texture metrics were evaluated under three predictor scenarios: (A) texture metrics only, (B) backscatter variables only, and (C) the combination of backscatter variables and texture metrics. Classification performance was evaluated for four machine learning algorithms: Random Forest (RF), Support Vector Machine (SVM), Generalized Linear Model (GLM), and Artificial Neural Network (ANN). Backscatter variables consistently outperformed texture metrics when used independently, demonstrating that radar backscatter captures the structural characteristics most relevant for vegetation fuel discrimination. However, integrating backscatter variables and texture metrics yielded the highest classification performance across all algorithms, demonstrating the complementary nature of these predictors sets. Among the evaluated models, SVM achieved the best overall performance (Accuracy = 0.560, Kappa = 0.414, Macro-F1 = 0.552). These results demonstrate that combining Sentinel-1 backscatter variables with texture metrics enhances the discrimination of structurally similar vegetation fuel classes and provides a robust, operational workflows for vegetation fuel mapping in Mediterranean ecosystems of central Chile.

Introduction

In recent decades, wildfires have emerged as one of the most significant disturbances affecting Mediterranean ecosystems and human communities, driven by increases in their frequency, spatial extent, and severity (Rita et al. 2020; Pausas and Keeley, 2021; Santelices-Moya et al. 2023; Gipouluo-Zuñiga et al. 2025). At the global scale, wildfires burn millions of hectares of vegetation annually, causing substantial alterations to landscape structure, biodiversity, and key ecosystem processes and functions (Cueto et al. 2025; Blanco-Rodríguez et al. 2025). In Chile, more than 99% of wildfires are human-caused and occur predominantly in the south-central part of the country (González et al. 2011). Since the onset of the prolonged megadrought in 2010, more than 1.89 million hectares have burned nationwide (CONAF, 2024; Ulibarry, 2025). This increasing wildfire activity poses a major threat to the Mediterranean ecosystems of central Chile, which are dominated by sclerophyllous forests and shrublands and are recognized as one of the world's biodiversity hotspots because of their high levels of endemism and the essential ecosystem services they provide (Otavo and Echeverría, 2017; Díaz et al. 2025). Within these ecosystems, wildfire occurrence is strongly influenced by anthropogenic pressures, land-use change, and increasing frequency of extreme weather conditions, all of which exacerbate ecosystem vulnerability and elevate wildfire risk (Jaque-Castillo et al. 2025; Kutchartt et al. 2025).

Vegetation fuels play a key role in wildfire dynamics, as their structure, composition, and moisture content directly influence ignition, fire propagation, and fire intensity (De Luis et al. 2004; Chhabra et al. 2022; Michael et al. 2022). However, accurately characterizing and classifying vegetation fuels remains challenging because of their structural complexity, spatial heterogeneity and the influence of topographic variability, particularly over large areas (Abdollahi and Yebra, 2023; Pérez-Ramírez et al. 2024). To support wildfire risk assessment and management, several fuel classification systems have been developed to represent the physical and structural properties of vegetation, including the fuel models proposed by Anderson (1982), Scott and Burgan (2005), and more recently adapted for European conditions by Aragoneses et al. (2023). In Chile, the KITRAL fuel classification system, developed by Julio et al. (1998), was specifically designed to characterize vegetation fuels under local environmental conditions, providing a standardized bases for wildfire risk assessment and management.

Remote sensing has become one of the principal tools for vegetation fuel mapping because it enables consistent observations over large spatial extents (Chuvieco et al. 2020). Nevertheless, optical imagery is often constrained by cloud cover, smoke, and varying illumination conditions, while spectral similarity among vegetation types can limit the discrimination of structurally similar fuels (Hoyer et al. 2026). In contrast, Synthetic Aperture Radar (SAR) imagery provides an attractive alternative, as microwave signals are sensitive to vegetation structure and moisture content while remaining largely unaffected by atmospheric conditions and solar illumination (Tanase et al. 2015; Gilić et al. 2023). Beyond radar backscatter, textural metrics derived from Grey Level Co-occurrence Matrices (GLCM), particularly Haralick features, capture the spatial organization and heterogeneity of vegetation. These metrics provide complementary structural information that enhances the characterization of vegetation fuel beyond the physical properties represented by SAR backscatter alone (Fan et al. 2024; Bhattacharjee and Gosh 2026).

Despite the demonstrated potential of SAR imagery for vegetation characterization, the combined use of Sentinel-1 backscatter variables and Haralick texture metrics for vegetation fuel classification remains poorly explored, particularly in structurally heterogeneous Mediterranean ecosystems such as those of central Chile. Previous studies have relied mostly on optical remote sensing (Stefanidou et al., 2018; Domingo et al., 2020) or have evaluated SAR backscatter and texture independently (Numbisi et al., 2019), with limited efforts to integrate these complementary sources of information within machine learning modelling frameworks. Consequently, the extent to which their combined use improves the discrimination of vegetation fuel types remains insufficiently understood.

This study aimed to classify vegetation fuel types defined under the KITRAL fuel classification system through the integration of Sentinel-1 SAR backscatter variables, Haralick texture metrics, and machine learning algorithms in Mediterranean ecosystems of central Chile. Specifically, the objectives were to: (i) characterize the structural response of vegetation fuel types using Sentinel-1 VV and VH backscatter signatures; (ii) evaluate the contribution of Haralick texture metrics derived from Sentinel-1 SAR imagery to the discrimination of vegetation fuel types; (iii) compare the performance of Random Forest (RF), Support Vector Machine (SVM), Artificial Neural Network (ANN), and multinomial Generalized Linear

Model (GLM) using different combinations of Sentinel-1 SAR backscatter variables and Haralick texture metrics to classify vegetation fuel types and identify areas with high biomass and combustion potential.

Material and Methods

2.1 Study area

The study area comprises 3 administrative regions in central Chile. These regions are characterized by a Mediterranean climate, with warm, dry summers and cold, wet winters (Fig. 1). Across the regions analysed, mean annual precipitation ranges from approximately 600 to 1,000 mm, with the highest values occurring in areas adjacent to the Andes Mountain Range. Mean temperatures range from approximately 8ºC in July to 20ºC in January, with the highest temperatures typically recorded in the central valley. Spatial variability in both precipitation and temperature is mostly driven by elevation and geographical location (AGRIMED 2017a, 2017b).

Vegetation in the study area is highly heterogeneous, comprising native sclerophyll forests, shrublands, grasslands, and exotic forest plantations. These vegetation formations differ substantially in canopy structure, biomass, vegetation density, and fuel continuity; generating contrasting radar backscatter responses (Fernández-Guisuraga et al, 2023). This pronounced structural heterogeneity provides an ideal setting for evaluating the potential of Sentinel-1 SAR imagery to discriminate vegetation fuel types.

2.2 Reference fuel dataset

Reference fuel data were obtained from the Community Prevention Network (CPN), a collaborative wildfire prevention initiative in central Chile that brings together forestry companies, local communities, and technical specialists to support vegetation fuel management and wildfire risk reduction. The CPN maintains an operational geospatial inventory of vegetation fuels developed through expert aerial photointerpretation and systematic field verification following the Chilean KITRAL fuel classification system. Owing to its standardized methodology and field validation, this inventory constitutes a ground-reference dataset for vegetation fuel mapping. The original database comprises multiple KITRAL fuel categories, which were aggregated into four classes for this study: native forest (NF), shrubland (S), grassland (GL), and forest plantations (FP). Following quality-control procedures, 3,645 reference fuel polygons were retained for subsequent analyses (Fig. 2a).

2.3 Radar backscatter signature

Sentinel-1 Ground Range Detected (GRD) images were obtained from the COPERNICUS/S1_GRD collection available in Google Earth Engine (Gorelick et al. 2017), (Fig. 2a). Images acquired in Interferometric Wide Swath (IW) mode, ascending orbit, dual polarization (VV and VH), and at spatial resolution of 10 m were selected between July and September 2021, corresponding to the winter–spring transition. To minimize topographic effects on radar backscatter, all images were radiometrically terrain-corrected to gamma-nought (γ°) using the terrain-flattening approach proposed by Vollrath et al. (2020).

Subsequently, a temporal median composite was generated separately for each polarization to reduce speckle noise and short-term temporal variability. Finally, the backscatter images were converted from decibel to linear scale and exported as GeoTIFF files in the UTM Zone 19S coordinate reference system (EPSG:32719).

Image processing was completed in R (R Core Team 2026), where raster datasets were harmonized with the reference polygons and cropped to the study area before feature extraction.

2.4 Backscatter characterization

Radar backscatter statistics were extracted for each reference fuel polygon using zonal statistics (Fig. 2b). For both VV and VH polarizations, the weighted mean, standard deviation, median, and interquartile values were calculated to characterize the backscatter response of each fuel type. Differences among fuel classes were evaluated independently for each polarization using the non-parametric Kruskal–Wallis test. When significant overall differences were detected, pairwise comparisons were performed using the Wilcoxon rank-sum test with Holm correction to account for multiple comparisons. Based on the observed discriminatory capacity of the two polarizations, the VH image was selected for subsequent texture analysis.

2.4 Extraction of Haralick texture metrics

Texture information was derived from the VH polarization using the Grey Level Co-occurrence Matrix (GLCM) originally proposed by Haralick et al. (1973) (Fig. 2c). GLCMs were computed using a 5 × 5 moving windows considering three spatial directions (0°, 45° and 90°). Texture calculations were restricted to a 250-m buffer surrounding each fuel polygon to minimize edge effects associated with incomplete moving windows. Six Haralick texture metrics commonly used in SAR image analysis were extracted: entropy, contrast, homogeneity, correlation, mean and energy (Zhang et al. 2017). These metrics describe complementary aspects of spatial organization, signal variability, and local heterogeneity within the radar response. For each polygon, texture statistics were extracted and incorporated into the classification database.

2.5 Variable Selection

The initial dataset consisted of 3,645 polygons distributed across four major fuel classes: native forest (NF = 305), shrubland (SB = 574), grasslands (GL = 1,174), and forest plantations (FP = 1,592). To address class imbalance, a random downsampling procedure was applied using the smallest class (NF, n = 305) as the reference level, thereby reducing potential classification bias associated with unequal class representation. After balancing, each fuel class contained 305 observations. The balanced dataset was then randomly divided into a training subset comprising 70% of the observations (n = 214 per class) and an independent test subset corresponding to the remaining 30% (n = 91 per class).

The predictor variables included Sentinel-1 SAR backscatter coefficients (VV and VH), the VV/VH backscatter ratio, and the Haralick texture metrics derived from the VH polarization. The VV/VH ratio was calculated as (Eq. 1):

$$Ratio\frac{VV}{VH} = \frac{\sigma^0 VV}{\sigma^0 VH}$$

Where $\sigma^0 VV$ is the radar backscatter coefficient (sigma naught) measured in the VV polarization, $\sigma^0 VH$ is the radar backscatter coefficient (sigma naught) measured in the VH polarization, and σ^0 represents the calibrated radar backscatter coefficient of the Sentinel-1 image. The textural dataset comprised six Haralick metrics calculated across three angular directions (0°, 45°, and 90°), resulting in eighteen texture variables. To explore the multivariate structure of these predictor variables, a Principal Component Analysis (PCA) was performed (Fig. 2d) to summarize the main patterns of variation among texture descriptors and facilitated the identification of relationships among variables. Variable redundancy was subsequently evaluated using Spearman's rank correlation coefficient, select because of its non-parametric properties and robustness to non-normal data distributions. The Spearman coefficient was calculated as (Eq. 2):

$$\rho = 1 - \frac{6\sum d_i^2}{n(n^2-1)}$$

Where ρ is Spearman's rank correlation coefficient, d_i is the difference between the ranks of the two variables for observation, n is the total number of paired observations and $\sum d_i^2$ is the sum of the squared differences between paired ranks. Based on the PCA and Spearman correlation analyses, a reduced predictor subset was defined by selecting variables with the greatest discriminatory capacity while minimizing redundancy. The final subset consisted of the VV and VH backscatter coefficients, the VV/VH ratio, and the five Haralick texture metrics: entropy (45°), homogeneity (45°), contrast (45°), mean (45°), and correlation (0°).

2.6 Supervised classification

To evaluate the contribution of SAR backscatter and Haralick texture variables to vegetation fuel discrimination, three classification scenarios were designed. Scenario A included only Haralick texture metrics derived from the VH polarization (Fig. 2e). Five texture descriptors were calculated for the three GLCM directions (0°, 45°, and 90°), resulting in a total of 15 predictor variables. Scenario B considered only the SAR backscatter variables, including the VV and VH polarizations and the VV/VH ratio. Finally, scenario C integrated both sources of information by combining the SAR backscatter variables with the Haralick texture metrics. For Scenarios A and C, two predictor configurations were evaluated. The first corresponded to the complete set of variables available for each scenario, whereas the second consisted of a reduced subset obtained from the PCA and Spearman correlation analyses. The selected subset comprised the VV and VH backscatter coefficients, the VV/VH ratio, and the Haralick texture metrics entropy (45°), homogeneity (45°), contrast (45°), mean (45°), and correlation (0°).

Four supervised machine learning algorithms were implemented to classify the vegetation fuel types: RF, SVM, multinomial GLM, and ANN based on a multilayer perceptron architecture. Model hyperparameters were optimized through repeated cross-validation using the *caret* package in R (Kuhn, 2024). Model

performance was assessed exclusively using the independent test dataset. Classification accuracy was evaluated using Overall Accuracy (OA), Cohen's Kappa coefficient, and Macro-F1 score, enabling comparison of both overall predictive performance and class-balanced classification accuracy across different classification scenarios and machine learning algorithms.

Results

A total of 3,645 vegetation fuel polygons were included in the analyses and grouped into four fuel classes according to the KITRAL fuel classification system: native forest (NF), forest plantation (FP), shrubland (SB), and grassland (GL) (Table 1). Forest plantations represented the dominant fuel class, accounting for 1,592 polygons (43.68%) and covering 35,016 ha (65.27% of the total study area).

Table 1
Number of reference fuel- types polygons and total area (ha) for each fuel class in the study according to the KITRAL fuel classification system.

Class	Nº Polygons	N° Polygons (%)	Area (ha)	Area (%)
Native forest	305	8,37	7.785	14.51
Forest plantation	1592	43.68	35.016	65.27
Shrubland	574	15.75	3.950	7.36
Grassland	1174	32.21	6.892	12.85
Total	3645	100.00	53.644	100.00

Grasslands constituted the second most abundant class, with 1,174 polygons (32.21%) and 6,892 ha (12.85%), followed by shrublands with 574 polygons (15.75%) and 3,950 ha (7.36%). Native forests were the least represented class, comprising 305 polygons (8.37%) and 7,785 ha (14.51%). Overall, the dataset exhibited an uneven distribution among fuel classes, with forest plantations representing the largest proportion of both the available polygons and the total mapped area.

The SAR backscatter response differed among fuel classes for both VV and VH polarizations (Fig. 3). Native forest consistently exhibited the highest backscatter values, whereas grassland showed the lowest response in both polarizations, particularly in VH. Shrubland and forest plantations displayed intermediate backscatter values, although both classes exhibited broader distributions than native forest and grassland.

Backscatter variability also differed among fuel classes. Native forest and grassland showed comparatively compact distributions, whereas shrubland and forest plantations presented wider interquartile ranges and longer whiskers, indicating greater within-class variability. This pattern was more pronounced in the VH polarization than in VV. Despite the general separation among fuel classes, partial overlap was observed between shrubland and forest plantations, particularly in the intermediate

backscatter range. Grassland remained clearly separated from native forest in both polarizations, while VH exhibited a larger contrast among fuel classes than VV.

The Kruskal - Wallis test confirmed the persistence of significant differences among NF, SB, GL, and FP in both polarizations. For VH, a value of $\chi^2 = 689.79$ with 3 degrees of freedom was obtained, showing a clear structural separation. In VV, although the statistic was lower—with $\chi^2 = 130.31$ and the same 3 degrees of freedom—the differences between fuel classes were also highly significant.

Given that the global test revealed statistically significant differences, pairwise comparisons were performed using the Wilcoxon test with Holm adjustment to control for multiple comparison errors (Fig. 4).

For both polarizations, comparisons between NF, GL, SB, and FP showed statistically significant differences ($p < 0.001$) in all cases for VH except between SB and FP for the VV polarization.

The PCA analysis of the backscatter and Haralick textures variables revealed that the first component (Dim1) explains 40.8% of the variability, while the second (Dim2) explains 24.9% (Fig. 5).

The variables contributing most to the factorial plane were VH, mean, VV, homogeneity, and contrast, with contribution values ranging from 15 to 25. In contrast, entropy, correlation, and the VV/VH ratio showed contributions of less than 10.

On Dim1, the variables VV, VH, mean, and homogeneity projected onto the positive semi-axis of the component, whereas contrast, entropy, and the VV/VH ratio fell toward negative values. On Dim2, homogeneity was the only variable projecting toward negative values, while correlation, contrast, entropy, VV, VH, and mean were located toward positive values.

Correlations among the same Haralick metric calculated at 0°, 45°, and 90° directions were classified as high to very high ($|\rho| \geq 0.70$). This pattern was also observed for entropy, mean, homogeneity, and correlation. In contrast, correlations between different metrics were primarily classified as low to moderate ($|\rho| < 0.70$), forming correlation blocks defined by each metric that were independent of the angular direction used. Consistent associations across the three evaluated directions were identified among the textural metrics. Entropy and homogeneity showed negative correlations classified as high ($\rho = -0.70$ to -0.80). Contrast exhibited positive correlations with homogeneity ($\rho = 0.66–0.80$) and negative correlations with entropy ($\rho = -0.58$ to -0.68). Meanwhile, mean showed positive correlations with correlation ($\rho = 0.71–0.86$), maintaining this pattern across all three directions.

Spectral variables displayed a pattern distinct from that of the textural metrics. VV and VH showed a correlation classified as high ($\rho = 0.81$), whereas the VV/VH ratio showed a high correlation with VV ($\rho = 0.86$) and a moderate negative correlation with VH ($\rho = -0.53$). In contrast, correlations between VV, VH, the VV/VH ratio, and the textural metrics were primarily classified as very low to low ($|\rho| < 0.50$), with no high correlations recorded between the two groups of variables.

The classification performance of the four machine learning algorithms under the three predictor scenarios is summarized in Table 2.

Table 2
Classification performance of Random Forest (RF), Support Vector Machine (SVM), Generalized Linear Model (GLM), and Artificial Neural Network (ANN) under the three predictor scenarios evaluated using Overall Accuracy, Cohen's Kappa and Macro-F1.

Scenario	Model	Accuracy	Kappa	Macro-F1
A	RF	0.46	0.28	0.46
A	SVM	0.48	0.29	0.46
A	GLM	0.41	0.21	0.46
A	NN	0.46	0.28	0.45
B	RF	0.47	0.29	0.46
B	SVM	0.52	0.36	0.47
B	GLM	0.50	0.33	0.48
B	NN	0.52	0.37	0.60
C	RF	0.55	0.40	0.54
C	SVM	0.56	0.41	0.55
C	GLM	0.53	0.38	0.53
C	NN	0.52	0.37	0.52

Overall, Scenario C, which combined Sentinel-1 backscatter variables and Haralick texture metrics, consistently achieved the highest performance across all evaluated models. Under this scenario, SVM produced the best overall results (Accuracy = 0.56, Kappa = 0.41, and Macro-F1 = 0.55), followed closely by RF (Accuracy = 0.55, Kappa = 0.402 and Macro-F1 = 0.54).

Scenario B, based only on backscatter variables, showed intermediate performance, with ANN reaching the highest Accuracy (0.52) and Kappa (0.37), whereas GLM obtained the highest Macro-F1 (0.48). In contrast, Scenario A, based exclusively on texture metrics, yielded the lowest classification performance for all evaluated algorithms, with SVM providing the highest Accuracy (0.48).

Discussion

The classification and spatial mapping of vegetation fuel types are fundamental for wildfire risk assessment and prevention, particularly in Mediterranean ecosystems where fire behaviour is strongly influenced by vegetation structure and composition (Bauer-Marschallinger et al. 2021; Millard et al. 2022;

Mueller et al. 2022; Ullmann et al. 2023; Cui et al. 2025). Our results demonstrate that Sentinel-1 SAR backscatter and Haralick texture metrics provide complementary information for discriminating vegetation fuel types under the Chilean KITRAL fuel classification system. The integration of both data sources consistently improved classification performance.

Sentinel-1 backscatter differed markedly among the four fuel classes. Native forest exhibited the highest VV and VH backscatter responses, whereas grasslands showed the lowest values, particularly in the cross-polarized VH channel. These differences are consistent with the contrasting vegetation structures of both fuel types. The multilayered canopy structure and higher biomass of native forests promote enhanced volumetric scattering, while the simpler and more homogeneous structure of grasslands favours surface scattering and reduce cross-polarized returns (Rüetschi et al. 2018; Pirotti et al. 2023).

A notable exception was the partial overlap between shrublands and forest plantations, particularly in the VV polarization, where post-hoc comparisons detected no significant differences. This likely reflects the structural similarity between dense shrublands and young or low-density *Pinus radiata* and *Eucalyptus* plantations, which produce comparable co-polarized scattering responses. In contrast, VH polarization provided greater discrimination, supporting previous studies that identify cross-polarized backscatter as more sensitive to differences in canopy architecture and volumetric scattering (Tanase et al. 2011; Fernández-Guisuraga et al. 2023; Pirotti et al. 2023; Paluba et al. 2025).

The multivariate analyses further supported these findings. The PCA showed that backscatter and texture variables captured different dimensions of vegetation structure rather than a single dominant pattern, while the low correlations observed between both variable groups indicate limited redundancy. Together, these results explain why combining SAR backscatter with Haralick texture metrics improved fuel discrimination compared with either predictor group alone.

The Spearman correlation analysis further supports the complementary nature of Sentinel-1 backscatter and Haralick texture metrics. While texture metrics showed high correlations across the three evaluated directions, correlations between backscatter and texture variables were generally weak, indicating that both predictor groups describe different aspects of vegetation fuels. Backscatter primarily reflects vegetation structural properties through radar scattering mechanisms, whereas texture metrics characterize the spatial organization and heterogeneity of the radar signal. This low redundancy between predictor groups explains the improved classification performance obtained when both sources of information were combined.

The comparison of the three predictor scenarios further highlights the contribution of each information source. Models based exclusively on Haralick texture metrics (Scenario A) consistently showed the lowest classification performance, indicating that spatial heterogeneity alone is insufficient to discriminate fuel classes with similar structural organization. Similar findings were reported by Caballero et al. (2020), who demonstrated that GLCM texture metrics improve Sentinel-1 classification when combined with radar backscatter rather than when used independently, supporting their role as complementary predictors rather than substitutes for SAR backscatter.

In contrast, models based only on Sentinel-1 backscatter variables (Scenario B) consistently outperformed texture-only models, confirming that VV, VH, and the VV/VH ratio capture the core structural information required for vegetation fuel discrimination. This finding agrees with the established sensitivity of VV and VH to surface, double-bounce, and volumetric scattering mechanisms, while the VV/VH ratio summarizes structural gradients related to biomass, canopy density, and vegetation complexity (Mandal et al. 2020; Jiao et al. 2022; Pradisty et al. 2025).

The highest classification performance was achieved when backscatter and texture variables were integrated (Scenario C), demonstrating that both predictor groups provide complementary information. While backscatter captures the physical interaction between the radar signal and vegetation structure, texture metrics describe the spatial heterogeneity of that response, resulting in a more complete representation of vegetation fuel characteristics than either predictor group alone.

Among the evaluated machine learning algorithms, SVM achieved the highest overall classification performance, closely followed by Random Forest, indicating that both methods effectively captured the non-linear relationships between SAR-derived predictors and vegetation fuel characteristics. In contrast, GLM consistently produced the lowest accuracies, reflecting the limitations of linear models when dealing with complex predictor-response relationships and interactions among variables (Gigović et al., 2019; Mansaray et al., 2019). The ability of SVM to construct optimal decision boundaries within transformed feature spaces makes it particularly suitable for separating vegetation classes characterized by continuous structural gradients rather than discrete class limits (Iqbal et al. 2021).

The comparison between the complete predictor set and the optimized subset further indicates that dimensionality reduction can reduce model complexity without substantially affecting classification performance. Retaining only the most informative variables decreased computational cost and the potential for overfitting while preserving the structural information required for vegetation fuel discrimination, supporting the development of scalable and reproducible Sentinel-1 classification workflows (Talukdar et al. 2020; Stromann et al. 2020).

Overall, the consistent improvement achieved by integrating Sentinel-1 backscatter and Haralick texture metrics demonstrates that both predictor groups provide complementary information for vegetation fuel classification. This combined approach offers a robust framework for operational fuel mapping under the Chilean KITRAL classification system in Mediterranean ecosystems.

Future research should explore the integration of SAR backscatter and texture-based predictors with spectral variables derived from passive optical sensors, such as Sentinel-2, to further improve fuel-type discrimination and classification accuracy.

Conclusions

This study demonstrated that Sentinel-1 SAR data provide an effective basis for vegetation fuel-type classification under the Chilean KITRAL system. Among the evaluated approaches, the integration of

SAR backscatter and texture metrics consistently improved classification performance, highlighting the complementary value of structural and spatial information for discriminating Mediterranean fuel types.

The results also showed that SVM and Random Forest were the most suitable machine learning algorithms for this application, suggesting that non-linear classifiers are particularly effective at exploiting the information content of SAR-derived predictors. These findings support the operational use of Sentinel-1 data for fuel mapping in Mediterranean ecosystems, where marked structural heterogeneity and the coexistence of multiple vegetation fuel types present important challenges for classification.

Future research should evaluate the integration of SAR backscatter and texture-based predictors with spectral information from passive optical sensors, such as Sentinel-2, to exploit the complementary structural and spectral characteristics of both data sources and further improve fuel-type discrimination and operational fuel mapping.

Declarations

The authors declare no competing interests

Funding

This research was supported by the Chilean National Agency for Research and Development (ANID) through the FONDEF project IT2310109, “Escalamiento de un sistema para el diseño de paisajes resistentes a incendios forestales integrando simulación, optimización e inteligencia artificial”. This work also received funding from the European Union’s Horizon 2020 Reserach and Innovation Programme under the Marie Sklodowska-Curie grant agreement Nº101007950.

Author Contribution

T.V.: Conceptualization, formal analysis, investigation, writing-original draft preparation; E.K.: Writing-review & editing; H.G.: Writing-review & editing, supervision; F.L.B.: Writing-review & editing, supervision; F.P.: Writing-review & editing; M.M. Conceptualization, writing-review &, supervision, funding acquisition.

Data Availability

The data used in this study are available from the corresponding author upon reasonable request.

References

1. Abdollahi A, Yebra M (2023) Forest fuel type classification: Review of remote sensing techniques, constraints and future trends. J Environ Manag 342:118315.

https://doi.org/10.1016/j.jenvman.2023.118315

2. AGRIMED (2017a) Atlas agroclimático de Chile. Estado actual y tendencias del clima. Tomo III: Regiones de Valparaíso, Metropolitana, O'Higgins y Maule. Universidad de Chile y Centro de Agricultura y Medioambiente. Santiago, Chile, p 208
3. AGRIMED (2017b) Atlas agroclimático de Chile. Estado actual y tendencias del clima. Tomo IV: Regiones del Biobío y de la Araucanía. Universidad de Chile y Centro de Agricultura y Medioambiente. Santiago, Chile, p 136
4. Anderson H (1982) Aids to determining fuel models for estimating fire behavior. US Department of Agriculture, Forest Service, Intermountain Forest and Range Experiment Station, Washington, DC, USA, p 26
5. Aragoneses E, García M, Salis M, Ribeiro LM, Chuvieco E (2023) Classification and mapping of European fuels using a hierarchical, multipurpose fuel classification system. Earth Syst Sci Data 15:1287–1315. https://doi.org/10.5194/essd-15-1287-2023
6. Bauer-Marschallinger B, Cao S, Navacchi C, Freeman V, Reuβ F, Geudtner D, Rommen B, Ceba Vega F, Snoeij P, Attema E, Reimer C, Wagner W (2021) The normalised Sentinel-1 Global Backscatter Model, mapping Earth's land surface with C-band microwaves. Sci Data 8:277. https://doi.org/10.1038/s41597-021-01059-7
7. Bhattacharjee AD, Ghosh N (2026) Texture Feature Analysis and Clustering of Remotely Sensed Data Using Gray-Level Co-occurrence Matrix and Haralick Features. In: Bansal JC, Saha S, Coello CAC, Rathore H (eds) Advances in Data-Driven Computing and Intelligent Systems. ADCIS 2024. Lecture Notes in Networks and Systems, vol 1445. Springer, Singapore. https://doi.org/10.1007/978-981-96-7140-3_19
8. Blanco-Rodríguez MA, Ameztegui A, Alday JG, Lecina-Diaz J, Pineda-Zapata S, Coll L (2025) Fire severity shapes landscape heterogeneity in Mediterranean forest ecosystems. Landsc Ecol 40:210. https://doi.org/10.1007/s10980-025-02198-7
9. Caballero GR, Platzeck G, Pezzola A, Casella A, Winschel C, Silva SS, Ludueña E, Pasqualotto N, Delegido J (2020) Assessment of Multi-Date Sentinel-1 Polarizations and GLCM Texture Features Capacity for Onion and Sunflower Classification in an Irrigated Valley: An Object Level Approach. Agronomy 10(6):845. https://doi.org/10.3390/agronomy10060845
10. Chhabra A, Rüdiger C, Yebra M, Jagdhuber T, Hilton J (2022) RADAR-Vegetation Structural Perpendicular Index (R-VSPI) for the Quantification of Wildfire Impact and Post-Fire Vegetation Recovery. Remote Sens 14(13):3132. https://doi.org/10.3390/rs14133132
11. Corporación Nacional Forestal (CONAF) (2024) Distribución nacional del daño (hectáreas) de incendios forestales según causalidad, 2003–2023
12. Chuvieco E, Aguado I, Salas J, García M, Yebra M, Oliva P (2020) Satellite Remote Sensing Contributions to Wildland Fire Since and Management. Curr Rep 6:81–96. https://doi.org/10.1007/s40725-020-00116-5

13. Cueto D, Alaniz A, Hidalgo-Corrotea C, Vergara P, Carvajal M, Barrios-Saravia A (2025) Chilean Mediterranean forest on the verge of collapse? Evidence from a comprehensive risk analysis. Sci Total Environ 964:178557. https://doi.org/10.1016/j.scitotenv.2025.178557
14. Cui L, Xu X, Chen S (2025) Estimating biomass consumption and carbon emissions by integrating GEDI, Sentinel-1, and Sentinel-2 data. Ecol Indic 178:113889. https://doi.org/10.1016/j.ecolind.2025.113889
15. De Luis M, Baeza MJ, Raventós J, González-Hidalgo JC (2004) Fuel characteristics and fire behaviour in mature Mediterranean gorse shrublands. Int J Wildland Fire 13(1):79–87. https://doi.org/10.1071/WF03005
16. Díaz IA, Armesto JJ, Godoy-Güinao J, Marcelo W, Mellado-Mansilla D, Moreno-González R, Ortega-Solis G, Peña C, Moreira R, Celis-Diez JL, Bustamante-Sanchez M (2025) Did Forests Exist in the Mediterranean Region of Santiago de Chile? The Discovery of a Remnant Patch of Closed-Canopy Forests with Large Trees. Austral Ecol 50(12):e70159. https://doi.org/10.1111/aec.70159
17. Domingo D, de la Riva J, Lamelas MT, García-Martín A, Ibarra P, Echeverría M, Hoffrén R (2020) Fuel type classification using airborne laser scanning and Sentinel-2 data in Mediterranean forest affected by wildfires. Remote Sens 12(21):3660. https://doi.org/10.3390/rs12213660
18. Fan J, Liu Y, Fan Y, Yao Y, Chen R, Bian M, Ma Y, Wang H, Feng H (2024) Estimation of potato leaf area index based on spectral information and Haralick textures from UAV hyperspectral images. Front Plant Sci 15:1492372. https://doi.org/10.3389/fpls.2024.1492372
19. Fernández-Guisuraga JM, Suárez-Seoane S, Calvo L (2023) Radar and multispectral remote sensing data accurately estimate vegetation vertical structure diversity as a fire resilience indicator. Remote Sens Ecol Conserv 9(1):117–132. https://doi.org/10.1002/rse2.299
20. Gigović L, Pourghasemi HR, Drobnjak S, Bai S (2019) Testing a new ensemble model based on SVM and random forest in forest fire susceptibility assessment and its mapping in Serbia's Tara National Park. Forests 10(5):408. https://doi.org/10.3390/f10050408
21. Gilić F, Gašparović M, Baučić M (2023) Current state and challenges in producing large-scale land cover maps: review based on recent land cover products. Geocarto Int 38(1):2242693. https://doi.org/10.1080/10106049.2023.2242693
22. Gipoulou- Zuñiga T, Rojas-Badilla M, LeQuesne C, Rozas V (2025) Endemic threatened tree species in the Mediterranean forests of central Chile are highly sensitive to ENSO-driven water availability and drought. Ecosyst 13:100324. https://doi.org/10.1016/j.fecs.2025.100324
23. González ME, Lara A, Urrutia R, Bosnich J (2011) Cambio climático y su impacto potencial en la ocurrencia de incendios forestales en la zona centro-sur de Chile (33º – 42º S). Bosque 32(3):215–219. http://dx.doi.org/10.4067/S0717-92002011000300002
24. Gorelick N, Hancher M, Dixon M, Ilyushchenko S, Thau D, Moore R (2017) Google Earth Engine: Planetary-scale geospatial analysis for everyone. Remote Sens Environ 202:18–27. http://dx.doi.org/10.1016/j.rse.2017.06.031

25. Haralick RM, Shanmugan K, Dinstein I (1973) Textural features for image classification. IEEE Trans Syst Man Cybern SMC –3(6):610–621. https://doi.org/10.1109/TSMC.1973.4309314
26. Hoyer S, Fluhrer A, Hellwing F, Harwin S, Krisp MJ, Jagdhuber T (2026) Assessing spatial scale effects in multi-sensor fire fuel mapping in the heterogeneous landscapes of Tasmania. Remote Sens Appl Soc Environ 42:101996. https://doi.org/10.1016/j.rsase.2026.101996
27. Iqbal N, Mumtaz R, Shafi U, Zaidi SMH (2021) Gray level co-occurrence matrix (GLCM) texture-based crop classification using low altitude remote sensing platforms. PeerJ Comput Sci 7:e536. https://doi.org/10.7717/peerj-cs.536
28. Jiao X, McNairn H, Yekkekhany B, Dingle Robertson L, Ihuoma S (2022) Integrating Sentinel-1 SAR and Sentinel-2 optical imagery with a crop structure dynamics model to track crop condition. Int J Remote Sens 43(22):6509–6537. https://doi.org/10.1080/01431161.2022.2142077
29. Jaque-Castillo E, Ojeda-Leal C, Muñoz-Berrios C (2025) The wildland-urban interface as no man's land in the construction of wildfire risk for Chilean coastal cities. Urbano 28(52):52–63. https://doi.org/10.22320/07183607.2025.28.52.04
30. Julio G, Pedernera P, Aguilera R (1998) Aplicaciones del SIG en la Gestión de la Protección contra Incendios Forestales – El Sistema KITRAL. Santiago, Chile: Actas Taller Regional FAO Aplicaciones de la Teledetección y los Sistemas de Información Geográfica a la Gestión Agrícola y del Medio Ambiente. FAO Chile
31. Kuhn M (2024) Caret: classification and regression training. R package version 7.0–1. http://CRAN.R-project.org/package=caret
32. Kutchartt E, Gayoso J, Guerra J, Pirotti F, Castagneri D, Matula R, Rojas Y, Olson ME, Zwanzig M (2025) Shrub aboveground biomass estimation considering bulk volume geometry: general and specific models for 14 species in the Mediterranean central Chile. New For 56:13. https://doi.org/10.1007/s11056-024-10081-7
33. Mandal D, Kumar V, Ratha D, Dey S, Bhattacharya A, Lopez-Sanchez JM, McNairn H, Rao YS (2020) Dual polarimetric radar vegetation index for crop growth monitoring using Sentinel-1 SAR data. Remote Sens Environ 247:111954. https://doi.org/10.1016/j.rse.2020.111954
34. Mansaray LR, Wang F, Huang J, Yang L, Kanu AS (2019) Accuracies of support vector machine and random forest in rice mapping with Sentinel-1A, Landsat-8 and Sentinel-2A datasets. Geocarto Int 35(10):1088–1108. https://doi.org/10.1080/10106049.2019.1568586
35. Michael Y, Kozokaro G, Brenner S, Lensky IM (2022) Improving WRF-Fire Wildfire Simulation Accuracy Using SAR and Time Series of Satellite-Based Vegetation Indices. Remote Sens 14(12):2941. https://doi.org/10.3390/rs14122941
36. Millard K, Darling S, Pelletier N, Schultz S (2022) Seasonally-decomposed Sentinel-1 backscatter time-series are useful indicators of peatland wildfire vulnerability. Remote Sens Environ 283:113329. https://doi.org/10.1016/j.rse.2022.113329 https://doi.org/10.1080/10106049.2021.1892209
37. Mueller MM, Dubois C, Jaghuber T, Hellwig FM, Pathe C, Schmullius C, Steele-Dunne S (2022) Sentinel-1 Backscatter Time Series for Characterization of Evapotranspiration Dynamics over

Temperate Coniferous Forests. Remote Sens 14:6384. https://doi.org/10.3390/rs14246384

38. Numbisi FN, Van Coillie FMB, De Wulf R (2019) Delineation of cocoa agroforests using multiseason Sentinel-1 SAR images: A low grey level range reduces uncertainties in GLCM texture-based mapping. ISPRS Int J Geo-Inf 8(4):179. https://doi.org/10.3390/ijgi8040179
39. Otavo S, Echeverría C (2017) Progressive fragmentation and loss of natural forests habitat in one of the global biodiversity hotspots. Rev Mex Biodivers 88:4. https://doi.org/10.1016/j.rmb.2017.10.041
40. Pradisty NA, Schlund M, Horstman EM, Willemen L (2025) Estimating canopy height and aboveground biomass in tropical mangrove restoration areas through multisource remote sensing. Ecol Inf 92:103522. https://doi.org/10.1016/j.ecoinf.2025.103522
41. Paluba D, Le Saux B, Sarti F, Stych P (2025) Identification of optimal Sentinel-2 SAR polarimetric parameters for forest monitoring in Czechia. AUC Geogr 60(1):46–60. https://doi.org/10.14712/23361980.2024.18
42. Pausas J, Keeley J (2021) Wildfires and global change. Front Ecol Environ 19(7):387–395. https://doi.org/10.1002/fee.2359
43. Pérez-Ramirez Y, Ferrat L, Filippi JB (2024) Wildland fire fuels database for Corsican - Mediterranean Forest stand types. Ecol Manag 565:122002. https://doi.org/10.1016/j.foreco.2024.122002
44. Pirotti F, Adedipe O, Leblon B (2023) Sentinel-1 Response to Canopy Moisture in Mediterranean Forests before and after Fire Events. Remote Sens 15(3):823. https://doi.org/10.3390/rs15030823
45. R Core Team (2026) R: A language and environment for statistics computing, version 4.6.1. The R project for statistical computing. Vienna, Austria. http://www.r-project.org/
46. Rita A, Camarero JJ, Nolè A, Borghetti M, Brunetti M, Pergola N, Serio C, Vicente-Serrano SM, Tramutoli V, Ripullone F (2020) The impact of drought spells on forests depends on site conditions: The case of 2017 summer heat wave in southern Europe. Glob Change Biol 26:851–863. https://doi.org/10.1111/gcb.14825
47. Rüetschi M, Schaepman ME, Small D (2018) Using Multitemporal Sentinel-1 C-band Backscatter to Monitor Phenology and Classify Deciduous and Coniferous Forests in Northern Switzerland. Remote Sens 10(1):55. https://doi.org/10.3390/rs10010055
48. Santelices-Moya R, Cabrera-Ariza A, Silva-Flores P, Ramos-Campos P (2023) Intra-specific variation in *Nothofagus alessandrii*, an endemic and endangered species of the Mediterranean forests of Chile. Bosque 44(2):315–327. https://dx.doi.org/10.4067/s0717-92002023000200315
49. Scott JH, Burgan R (2005) Standard fire behavior fuel models: a comprehensive set for use with Rothermel's surface fire spread model. General Technical Report RMRS-GTR-153, USDA Forest Service, Rocky Mountain Research Station, Fort Collins, CO, USA, p. 72
50. Stefanidou A, Gitas IZ, Katagis T (2018) Fuel type mapping using object-based image analysis of DMC and Landsat-8 OLI imagery. Geocarto Int 33(10):1060–1075. https://doi.org/10.1080/10106049.2017.1333532
51. Stromann O, Nascetti A, Yousif O, Ban Y (2020) Dimensionality reduction and feature selection for object-based land cover classification based on Sentinel-1 and Sentinel-2 time series using Google

Earth Engine. Remote Sens 12:76. https://doi.org/10.3390/rs12010076

52. Talukdar S, Singha P, Mahato S, Pal S, Liou YA, Rahman A, Ali MA (2020) Land-use land-cover classification by machine learning classifiers for satellite observations—A review. Remote Sens 12:1135. https://doi.org/10.3390/rs12071135
53. Tanase MA, Kennedy R, Aponte C (2015) Radar Burn Ratio for fire severity estimation at canopy level: An example for temperate forests. Remote Sens Environ 170:14–31. https://doi.org/10.1016/j.rse.2015.08.025
54. Ulibarry P (2025) Incendios Forestales. Período 2019–2024. Biblioteca del Congreso Nacional de Chile. Santiago, Chile, p 4
55. Ullmann T, Jaghuber T, Hoffmeister D, May SM, Baumhauer R, Bubenzer O (2023) Exploring Sentinel-1 backscatter time series over the Atacama Desert (Chile) for seasonal dynamics of surface soil moisture. Remote Sens Environ 285:113413. https://doi.org/10.1016/j.rse.2022.113413
56. Vollrath A, Mulligan M, Reiche J (2020) Angular-based radiometric slope correction for Sentinel-1 on Google Earth Engine. Remote Sens 12:1867. https://doi.org/10.3390/rs12111867
57. Zhang X, Cui J, Wang W, Lin C (2017) A Study for Texture Feature Extraction of High-Resolution Satellite Images Based on a Direction Measure and Gray Level Co-Occurrence Matrix Fusion Algorithm. Sensors 17(7):1474. https://doi.org/10.3390/s17071474

Figures

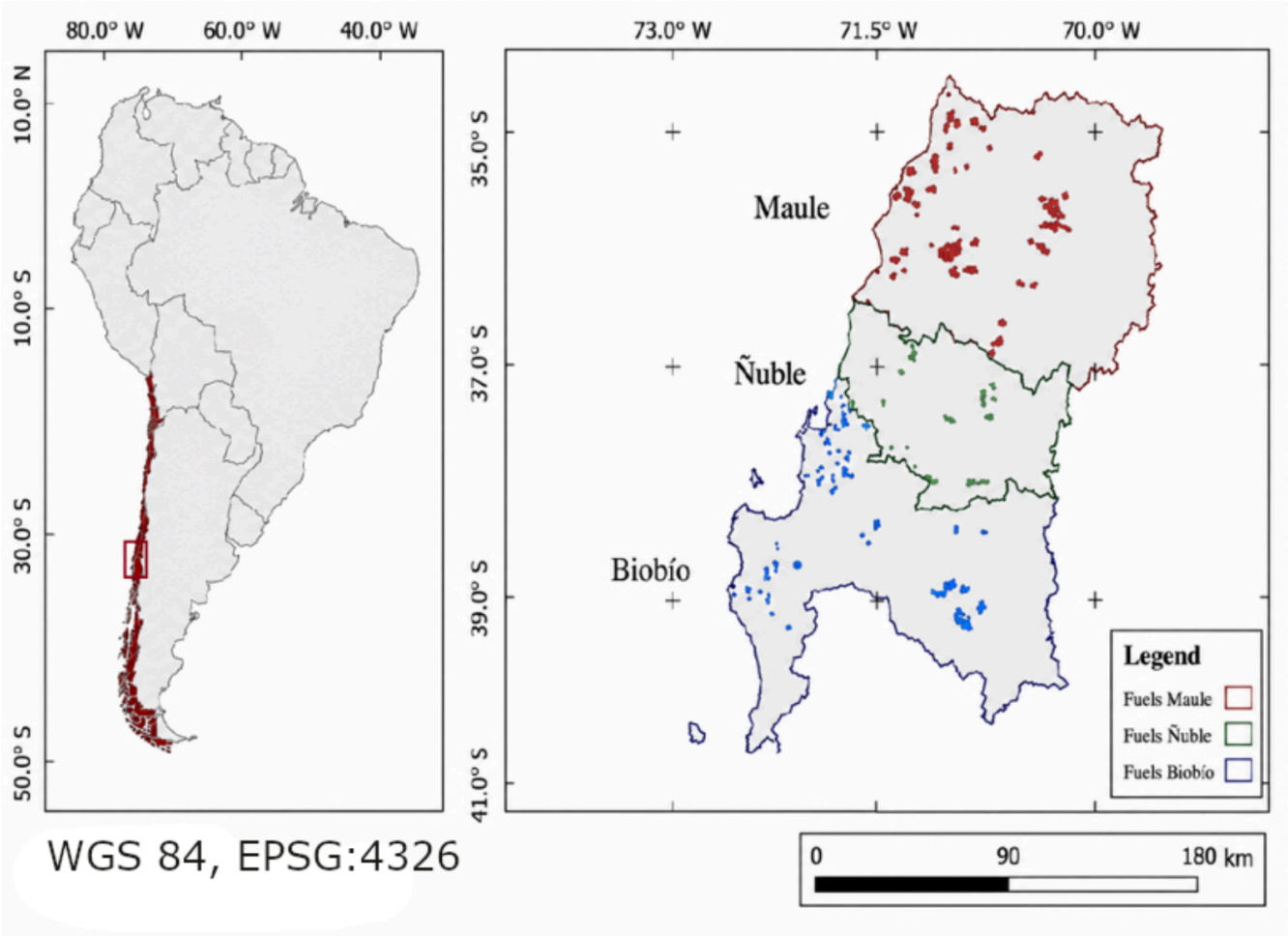


Figure 1

Location of the study area within central Chile.

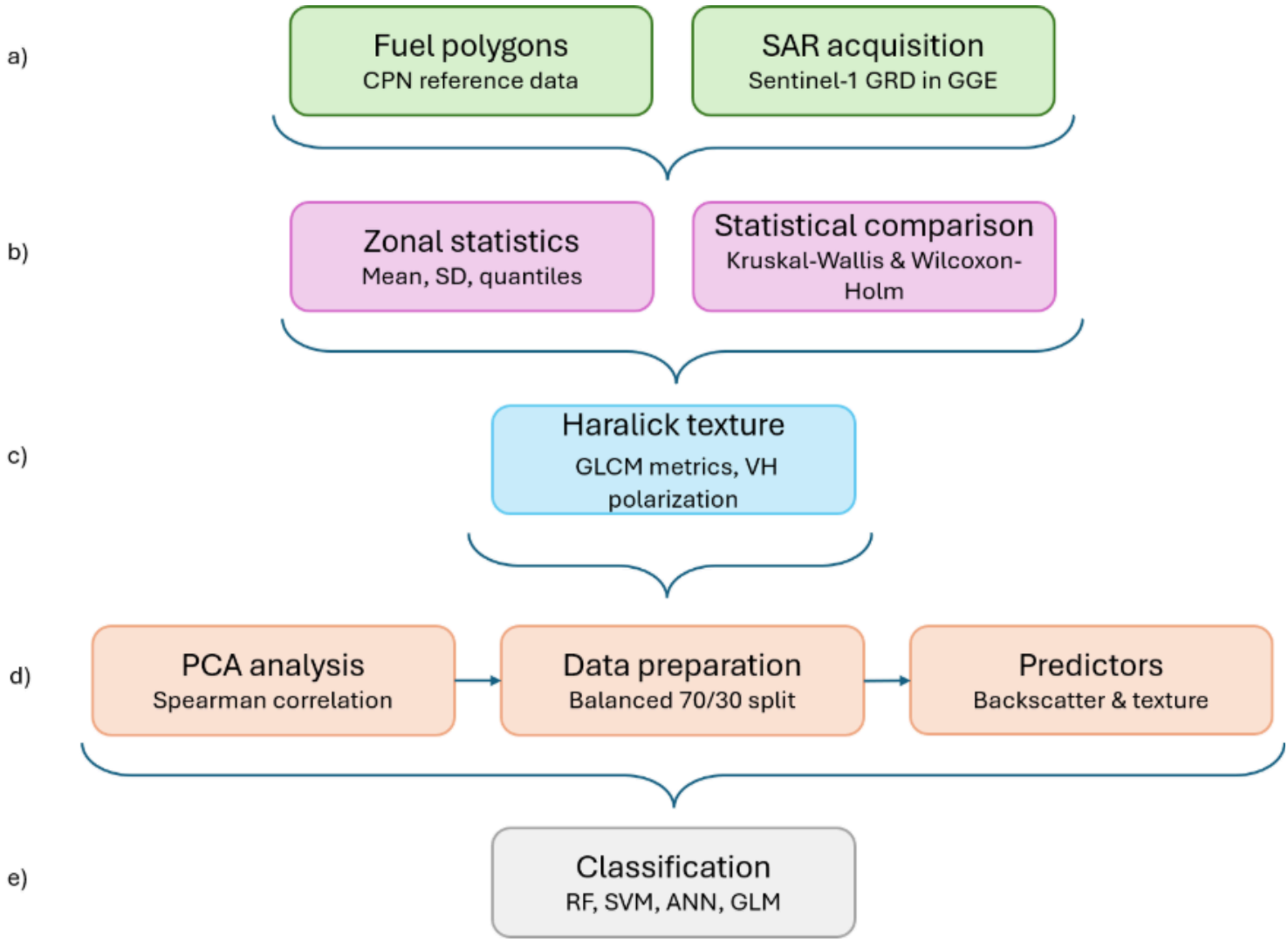


Figure 2

Overall workflow of the study, illustrating data acquisition, preprocessing, feature extraction, and machine learning model evaluation using supervised classification metrics and fuel-type polygons as ground truth data.

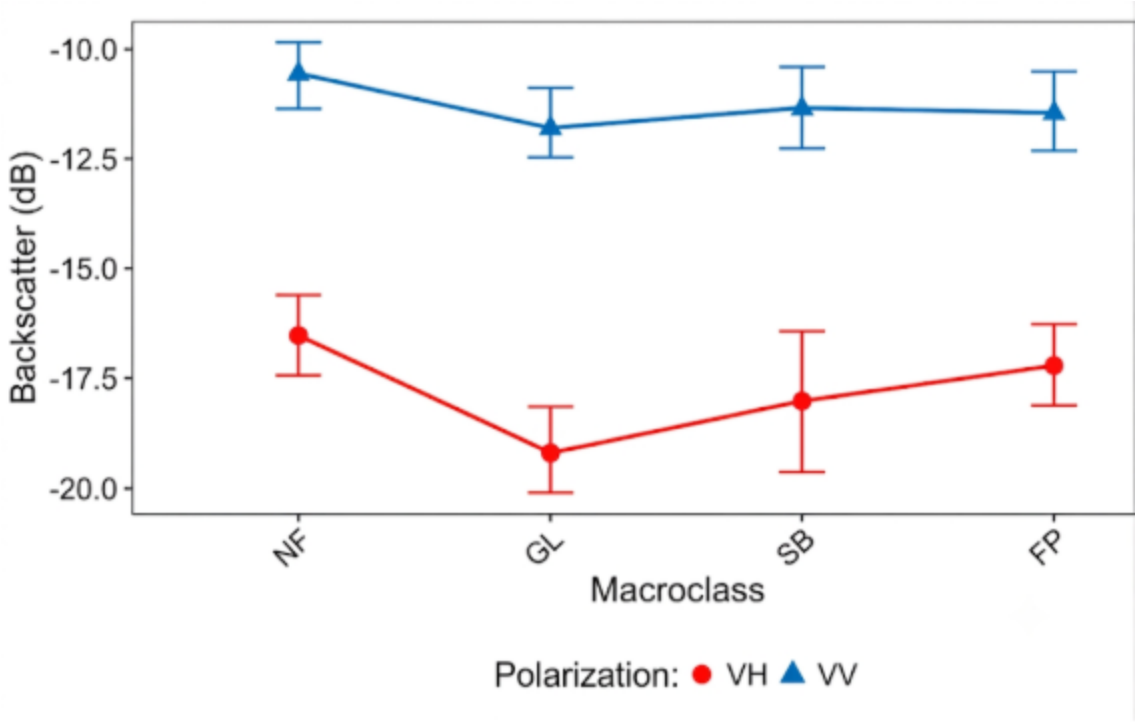


Figure 3

Boxplots for SAR backscatter signatures of the four vegetation fuel classes (native forest, forest plantation, shrubland and grassland) derived from Sentinel-1 VV and VH polarizations. Boxes represent the interquartile range (IQR), the central line indicates the median, whiskers extend to 1.5 × IQR, and points correspond to outliers.

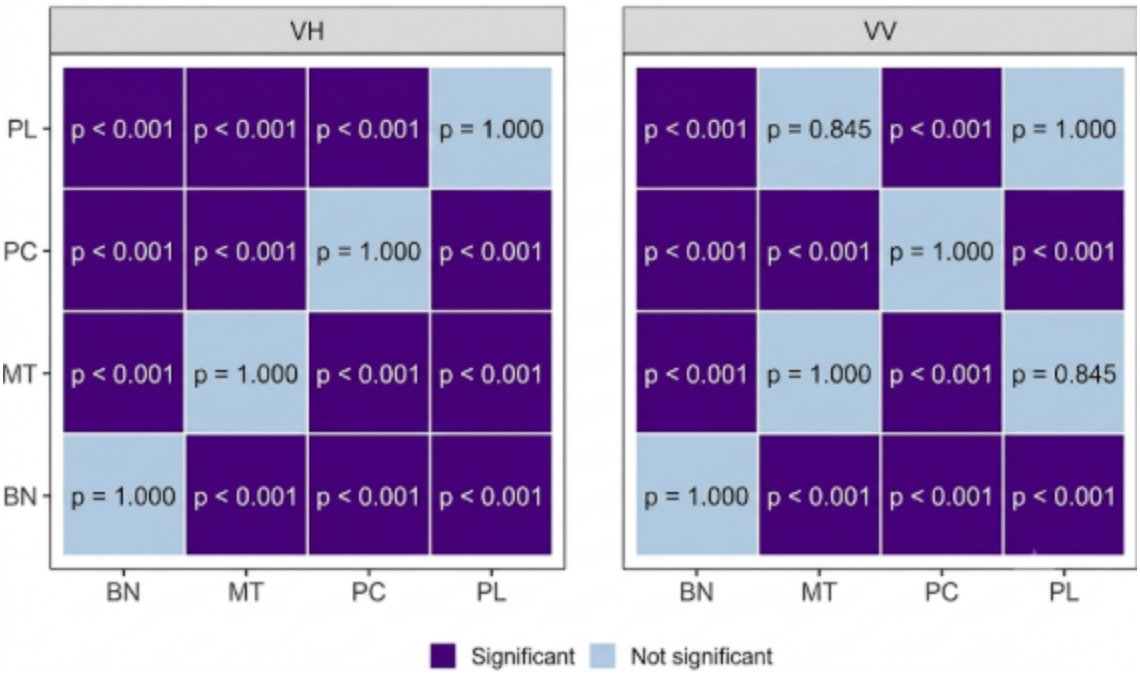


Figure 4

Pairwise Wilcoxon post-hoc comparisons among vegetation fuel classes for Sentinel-1 VH and VV backscatter following the Kruskal–Wallis test. Significant differences are indicated according to Holm-adjusted p-values.

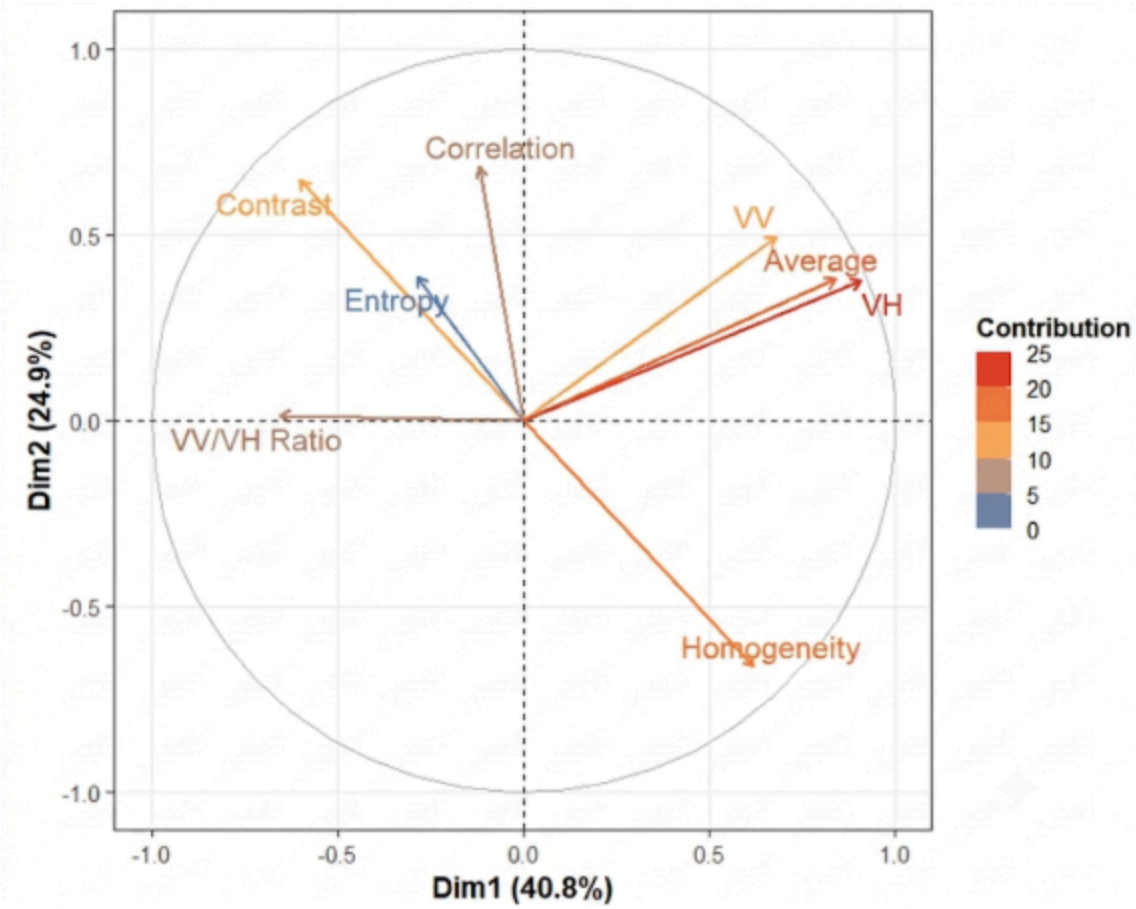


Figure 5

Principal Component Analysis (PCA) of backscatter and Haralick texture metrics derived from the Sentinel-1 VH polarization. (a) PCA score plot showing the distribution of vegetation fuel classes. (b) Correlation circle displaying the contribution and orientation of texture variables with respect to the first two principal components.

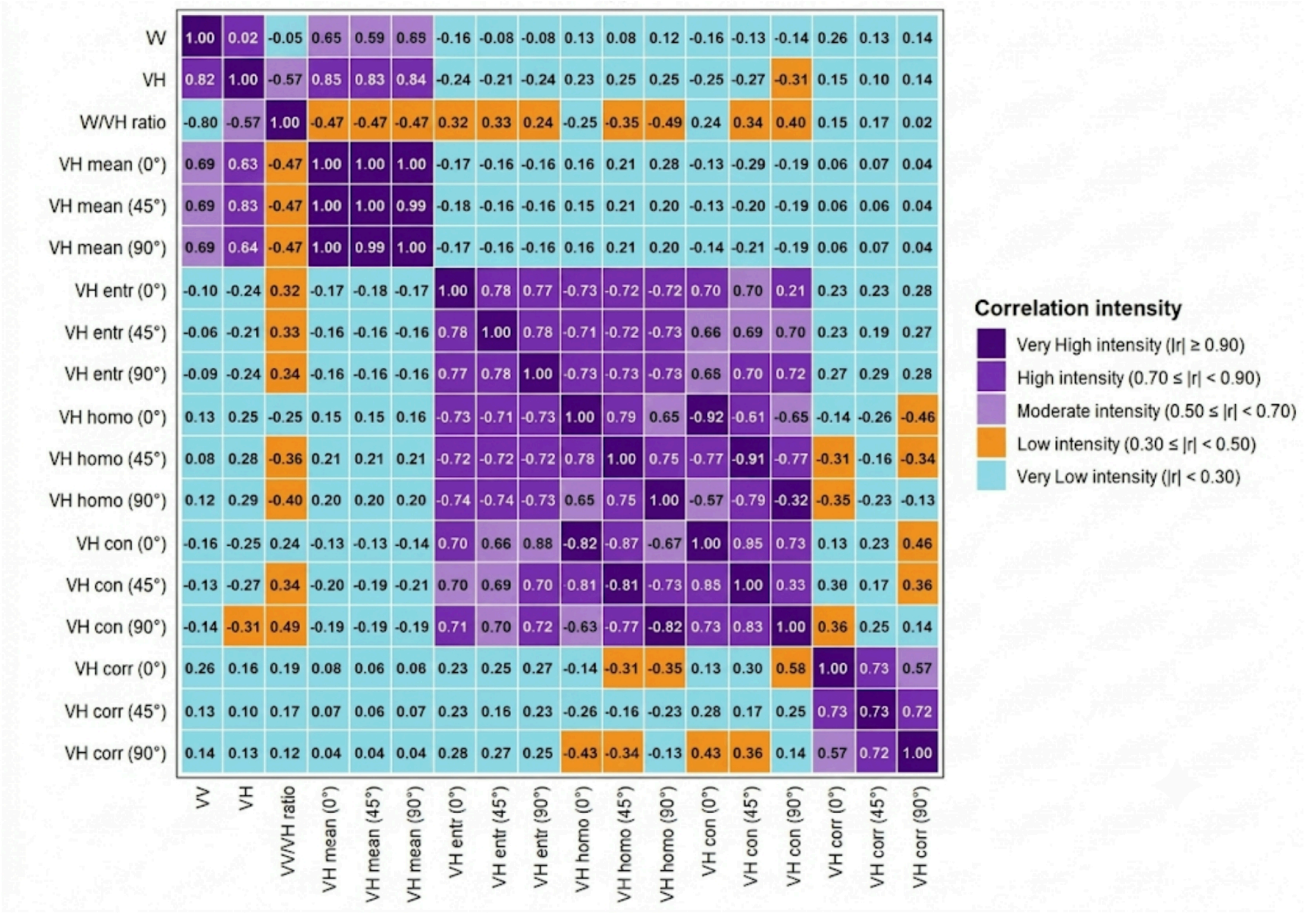


Figure 6

Spearman correlation matrix of Sentinel-1 backscatter variables and Haralick texture metrics. Colours represent the magnitude and direction of the correlation coefficients. Corr =correlation, con = contrast, entr = entropy, homo = homogenenidad.